NATIONAL ADVISORY COMMITTEE FOR AERONAUTICS

TECHNICAL NOTE 2177

LOW-SPEED CHARACTERISTICS OF FOUR CAMBERED, 10-PERCENT-THICK NACA AIRFOIL SECTIONS

By George B. McCullough and William M. Haire

Ames Aeronautical Laboratory
Moffett Field, Calif.

Washington
August 1950

NATIONAL ADVISORY COMMITTEE FOR AERONAUTICS

TECHNICAL NOTE 2177

LOW-SPEED CHARACTERISTICS OF FOUR CAMBERED, 10-PERCENT-THICK NACA AIRFOIL SECTIONS

By George B. McCullough and William M. Haire

SUMMARY

A two-dimensional low-speed investigation was made of four thin, cambered airfoil sections. The airfoil sections were the NACA 64A310, a = 1.0; the 64A810, a = 0.8 (modified); and the NACA 0010 cambered to the same two mean lines. The data, obtained for Reynolds numbers of 3.7×10^6 and 5.2×10^6, include measurements of lift, drag, pitching moment, and chordwise distribution of pressure. The effect of surface roughness was investigated as well as the effect of a split flap deflected 60°.

It was found that the NACA four-digit-series sections developed greater maximum lift than the corresponding NACA 64A-series sections for all test conditions. The maximum lifts of both series without flaps were reduced by surface roughness; the effect was greater for the sections with the smaller amount of camber. The increment of maximum lift produced by the split flap deflected 60° was greater for the NACA four-digit-series sections.

Visual observation of tufts attached to the upper surfaces of the models indicated that the stall of the sections cambered for an ideal lift coefficient of 0.3 was the result of separation of flow from the leading edge almost immediately after the appearance of turbulent separation at the trailing edge; whereas, for the sections cambered for an ideal lift coefficient of 0.8, turbulent separation from the trailing edge progressed as far forward as the 70-percent-chord station before laminar separation appeared near the leading edge.

INTRODUCTION

As part of a general study of the stalling characteristics of thin wings, a two-dimensional investigation was made of the effect of a large change of airfoil thickness distribution on the low-speed stalling characteristics of cambered airfoil sections. Specifically, the basic thickness distributions compared were 10-percent-thick NACA four-digit and 64A-series sections. Calculations based on the method described in reference 1 indicate that differences in the high-speed characteristics of symmetrical conventional and low-drag airfoil sections tend to disappear when

these sections are cambered by combining them with the same NACA a--type mean line. If there is little or no difference between the two types of cambered airfoil sections from the standpoint of high-speed drag, the choice of section for aircraft employing cambered wings probably will depend on the low-speed stalling characteristics. For this reason, it seemed desirable to compare the characteristics of typical sections at low speed.

The models employed for the investigations were cambered for ideal lift coefficients of 0.3 and 0.8, thereby enabling comparisons of the two sections to be made for two fairly widely separated amounts of camber. The mean lines were the same for each pair of models with the same amount of camber, but differed for the two amounts of camber.

The data obtained include measurements of lift, drag, pitching moment, the chordwise distribution of pressure, and visual studies of the character of the stall as indicated by tufts of thread attached to the upper surfaces of the models. Data were obtained for the models in the smooth condition and with roughness applied to the forward 8 percent of the chord, both with and without a simulated split flap deflected 60°.

The investigation was conducted in the Ames 7- by 10-foot wind tunnel No. 1.

NOTATION

The data are presented in the form of standard NACA coefficients defined as follows:

c_{d_o} section profile-drag coefficient $\left(\frac{D_o}{qc}\right)$

c_l section lift coefficient $\left(\frac{L}{qc}\right)$

c_{l_i} design section lift coefficient

$c_{l_{max}}$ maximum section lift coefficient

c_m section pitching-moment coefficient, referred to the quarter-chord point $\left(\frac{M}{qc^2}\right)$

a mean-line designation, fraction of chord over which design load is uniform

c airfoil chord, feet

D_o profile drag per unit span, pounds per foot

H_o free-stream total pressure, pounds per square foot

L lift per unit span, pounds per foot

M pitching moment relative to the quarter-chord point per unit span, pound-feet per foot

p local static pressure, pounds per square foot

q free-stream dynamic pressure, pounds per square foot

R Reynolds number, based on airfoil chord

S pressure coefficient $\left(\frac{H_o - p}{q}\right)$

x chordwise station, feet

α_o section angle of attack, degrees

α_1 section angle of attack corresponding to design lift coefficient, degrees

δ_f deflection of trailing-edge split flap from lower surface, degrees

MODELS

Four models, each of 4-foot chord, were constructed of wood and differed from one another only in airfoil section. When mounted in the wind tunnel, each model spanned the 7-foot dimension. Attached to the ends of the models were circular plates, 6 feet in diameter, which formed part of the tunnel floor and ceiling. To permit the measurement of pressure distributions, flush-type pressure orifices were provided along the midspan sections of the models. The airfoil-section designations were as follows:

NACA 64A310, a=1.0[1]

NACA 0010, a=1.0, $c_{l_i} = 0.3$

NACA 64A810, a=0.8 (modified)[1]

NACA 0010, a=0.8 (modified), $c_{l_i}=0.8$

[1]Characteristics of the a=1.0 mean line are given in reference 2 and of the a=0.8 (modified) mean line in reference 3.

Coordinates of the four sections are given in table I and sketches of the profiles in figure 1.

The effect of a 20-percent-chord split flap, hinged on the lower surface, was simulated by attaching a flat steel plate to the lower surface of the model with 60° wooden brackets. The same brackets were used with all four models so that the 60° flap deflection was maintained with respect to the lower surface in all cases.

Roughness consisting of carborundum grains of approximately 0.011-inch diameter was applied to the upper and lower surfaces for a distance of 8 percent of the chord rearward from the leading edge of the model. The grains were distributed so as to cover approximately 15 to 20 percent of this area.

TESTS

The test data were obtained for two values of Reynolds number: 3.7×10^6 and 5.2×10^6, which corresponded to Mach numbers of 0.131 and 0.187, respectively. Tests were made for both values of Reynolds number for the models in the smooth condition, and for the higher value ($R = 5.2 \times 10^6$) with roughness applied to the leading-edge regions.

Force measurements of lift and pitching moment were made with the wind-tunnel balance system. Except where noted otherwise, the data were corrected for the effects of tunnel-wall constraint and compressibility by the methods outlined in reference 4.

RESULTS AND DISCUSSION

Lift

The lift and moment characteristics of the four models as measured by the wind-tunnel balance system are shown in figures 2 and 3. For all test conditions, both without and with the simulated split flap, greater maximum section lift coefficients were obtained for the NACA four-digit-series airfoils than for the corresponding NACA 64A-series airfoils. For the airfoils cambered for a design lift coefficient of 0.3, $c_{l_{max}}$ for the four-digit airfoil was greater by about 0.2. The superiority of the four-digit series diminished when the camber was increased to that for a design lift coefficient of 0.8. For this amount of camber the increment of maximum lift coefficient was less than 0.1.

The lift characteristics of the four airfoils are summarized in the following table:

Surface condition	Smooth $R = 3.7 \times 10^6$		Smooth $R = 5.2 \times 10^6$		Rough $R = 5.2 \times 10^6$	
Airfoil	64A310	0010 c_{l_i}=0.3	64A310	0010 c_{l_i}=0.3	64A310	0010 c_{l_i}=0.3
$c_{l_{max}}$	1.32	1.53	1.33	1.53	1.12	1.36
$dc_l/d\alpha_o$	.108	.108	.109	.109	.110	.109
$c_{l_{max}}$ with $\delta_f = 60^\circ$	1.85	2.37	1.92	2.36	1.98	2.20
Airfoil	64A810	0010 c_{l_i}=0.8	64A810	0010 c_{l_i}=0.8	64A810	0010 c_{l_i}=0.8
$c_{l_{max}}$	1.68	1.76	1.70	1.74	1.62	1.69
$dc_l/d\alpha_o$	.104	.104	.107	.107	.104	.103
$c_{l_{max}}$ with $\delta_f = 60^\circ$	2.39	2.62	2.43	2.66	2.41	2.53

The values given for the lift-curve slope were measured at the design lift coefficient.

In order to provide a check on the wind-tunnel balance measurements, the section lift coefficients in the vicinity of the maximum lift of the smooth models were computed by integration of the pressure distributions. The values so determined were about 0.02 greater than those determined from the balance system except for the four-digit-series section cambered for c_{l_i}=0.8. For this section, $c_{l_{max}}$ was 0.1 greater than the balance-system value.

The increment of maximum lift produced by the simulated split flap was greater for the four-digit-series airfoils than for the 64A series, and for both series the increment of maximum lift produced by the flap was greater for the more highly cambered sections.

The addition of roughness to the unflapped airfoils reduced the maximum lift coefficient about 0.2 for the airfoils cambered for c_{l_i}=0.3, and less than 0.1 for the airfoils cambered for c_{l_i}=0.8. For the airfoils with the simulated split flap, the application of leading-edge roughness produced a different effect on each series of airfoils. For the 64A310 airfoil the maximum lift was increased, and for the 64A810 airfoil the maximum lift was decreased; whereas, for the four-digit series with either amount of camber, the maximum lift coefficient was decreased more than 0.1.

Visual studies of the stall patterns, as indicated by tufts, showed that the flow over the models was unsteady near maximum lift. In general, both the models cambered for $c_{l_i}=0.3$ stalled from flow separation at the leading edge almost immediately after the appearance of turbulent separation at the trailing edge. The models cambered for $c_{l_i}=0.8$ stalled primarily from turbulent separation. The area of separated flow progressed forward to about the 70-percent-chord station before the stall pattern became confused by small areas of laminar separation near the leading edge. These stalling characteristics were also indicated by the pressure distributions (not presented) obtained for angles of attack greater than those corresponding to maximum lift. For the sections cambered for $c_{l_i}=0.3$, the peak negative pressures collapsed abruptly at maximum lift; whereas, for the sections cambered for $c_{l_i}=0.8$, the collapse of the peak negative pressure was gradual. The pressure distribution near the trailing edges of the latter sections were relatively flat, indicative of turbulent separation. Within the range of the investigation ($R = 3.7 \times 10^6$ to 5.2×10^6), the stalling characteristics of all the four airfoil sections were relatively unaffected by Reynolds number.

The reason for the more deleterious effects of roughness on the maximum lift of the sections of lower camber may be explained as follows: An unpublished result of an investigation of the stalling characteristics of the NACA 63-009 airfoil section was that roughness on the upper surface reduced maximum lift, but roughness on the lower surface increased maximum lift. Hence, it may be inferred that, for a region where the flow is laminar and where there is a severe adverse pressure gradient, surface roughness tends to promote early separation of the boundary layer. Since the sections cambered for $c_{l_i}=0.3$ stalled primarily from laminar separation, it would be expected from the foregoing reasoning that roughness would have a more adverse effect on these sections than on the sections cambered for $c_{l_i}=0.8$, which stalled primarily from turbulent separation.

As can be seen in figures 3(a) and 3(b), the lift curve of the NACA 64A810 section departs from that of the four-digit-series section as the negative-lift range is approached from the positive side. Coincident with the shift in the lift curve is a strong positive trend of the pitching moment. The shift of the lift curve is thought to be produced by a localized region of laminar-separated flow on the lower surface followed by reattachment. Lower-surface pressure distributions shown in figure 4 support this belief. For an angle of attack of -5.2°, immediately prior to the force break, there is a strong negative pressure peak near the leading edge followed by a severe pressure gradient. For an angle of attack of -5.7°, the negative pressure peak has collapsed and there is a considerable chordwise extent of substantially constant pressure. A similar abrupt redistribution of pressure occurred for the NACA 64A006 airfoil section for an angle of attack between 4.5° and 5° (reference 5). It was shown that the collapse of the peak pressures was accompanied by the appearance near the leading edge of a region of separated flow which subsequently reattached to

the surface and progressed downstream as a thick, turbulent boundary layer. The collapse of the pressure peak on the NACA 64A006 airfoil also was accompanied by discontinuities in the force and moment characteristics.

With roughness on the surface (fig. 3(c)), the lift and moment characteristics of the two sections cambered for $c_{l_i}=0.8$ are in good agreement throughout the entire lift range. The pitching moments of both sections show a positive trend in the negative-lift range similar to that of the smooth NACA 64A810 section (fig. 3(b)). By analogy, it is evident that a localized region of laminar separated flow formed on the lower surface of the roughened four-digit-series section prior to the attainment of the maximum negative-lift coefficient. However, for the two roughened sections, the extent of the region of separated flow increased more gradually with increasingly negative angle of attack than for the smooth NACA 64A810 section. These characteristics were borne out by inspection of the pressure distributions and the balance-system measurements of drag.

The slopes of the lift curves at the design lift coefficient for the models cambered for $c_{l_i}=0.3$ were not appreciably affected by Reynolds number or by the addition of roughness. However, for the models cambered for $c_{l_i}=0.8$, the slopes of the lift curves were reduced from 0.107 per degree to 0.104 per degree by a reduction of the Reynolds number from 5.2×10^6 to 3.7×10^6. A similar decrease in lift-curve slope was produced by the addition of surface roughness.

The greater sensitivity of the more highly cambered sections to Reynolds number and surface roughness may be explained by consideration of the factors which influence boundary-layer growth. For conditions corresponding to design lift, the adverse pressure gradients over the rear portions of the models cambered for $c_{l_i}=0.3$ were relatively mild, and as a result the boundary layers were thin and had no tendency to separate. For the models cambered for $c_{l_i}=0.8$, because of their greater design lift coefficient, the adverse pressure gradients were more severe and caused a more rapid boundary-layer growth. These boundary layers had developed to a stage where they were about to thicken rapidly as is shown by the nonlinearity of the lift curves above the design lift coefficient, and as a consequence were more sensitive to any circumstance adverse to boundary-layer flow. For this reason, reduction of Reynolds number or the addition of surface roughness reduced the lift-curve slope of the models cambered for $c_{l_i}=0.8$.

Pitching Moment

The magnitudes of the pitching-moment coefficients are about what would be expected from examination of data for airfoil sections having camber lines similar to those tested. However, the variation of the pitching-moment coefficient with lift coefficient (figs. 2 and 3) shows a

positive trend beyond the stall; data for similar airfoil sections from other sources show the opposite trend. The reason for this is not understood. Integration of the pressure distributions also showed positive trends which were less pronounced than those shown by the force measurements.

Drag

The drag coefficients computed from wake surveys behind the four models are shown in figure 5. The minimum section profile-drag coefficients and the corresponding values of the section lift coefficient for a Reynolds number of 5.2×10^6 are tabulated as follows:

Airfoil section	Surface condition			
	Smooth		Rough	
	$c_{d_{o_{min}}}$	c_l	$c_{d_{o_{min}}}$	c_l
64A310	0.0042	0.3	0.0082	0.2
0010 $c_{l_i}=0.3$	.0051	.2	.0084	.2
64A810	.0048	.8	.0087	.4
0010 $c_{l_i}=0.8$	.0055	.4	.0088	.4

The minimum drags of the 64A-series airfoils, as would be expected, were less than those of the corresponding four-digit-series airfoils for all test conditions. The minimum drags and the centers of the low-drag ranges of the smooth 64A-series airfoils occurred for lift coefficients close to the design values. The minimum drags of the four-digit-series airfoils occurred for lift coefficients considerably lower than the design values.

The effect of increased camber was to increase the drag corresponding to the design lift of both the 64A- and the four-digit-series airfoils. The low-drag range of the 64A-series airfoil became less well defined and of smaller extent with increased camber.

The effect of Reynolds number on minimum drag was inappreciable for all the airfoils, but increasing the Reynolds number reduced the drag outside the low-drag range.

The addition of surface roughness, of course, increased the drag in all cases and completely removed the low-drag "bucket" of the 64A-series. The minimum drag of the rough 64A-series sections occurred for the same values of lift coefficient as for the four-digit series.

Pressure Distribution

Experimental pressure distributions corresponding to three conditions, one near zero lift, one near design lift, and one near maximum lift, are shown for the four airfoils in figure 6. These data have not been corrected for the effects of tunnel-wall constraint or compressibility. The pressure distributions of the two airfoils cambered for $c_{l_i}=0.3$ (fig. 6(a)) do not indicate any flow separation near maximum lift; whereas those of the airfoils cambered for $c_{l_i}=0.8$ indicate turbulent separation over the rear 20 percent of the chord (fig. 6(b)). In all respects the pressure distributions are typical of the two types of airfoil sections and no unexpected abnormalities are revealed.

Comparisons of the theoretical and experimental pressure distributions corresponding to the design values of lift are shown in figure 7. The theoretical pressure distributions were derived by the method of velocity superposition described in reference 2, and the experimental pressure distributions were obtained from data measured on either side of the design lift coefficient. The experimental data are for a Reynolds number of 5.2×10^6 and are corrected for the effects of tunnel-wall constraint and compressibility by the method of reference 4.

As is pointed out in reference 2, the method of velocity superposition gives pressure distributions which correspond to lift coefficients greater than the design values by an amount dependent on the thickness ratio of the basic thickness form. (In the present case the amount was about 10 percent.) Both the theoretical and experimental pressure distributions were adjusted by interpolation until the values of lift coefficient obtained by integration of the pressure diagrams agreed closely with the design values. The section angles of attack α_i shown in figure 7 are those corresponding to the adjusted pressure diagrams. (As is also mentioned in reference 2, the theoretical angles of attack are only approximately correct and should not be used where great accuracy is required without experimental verification.)

In general, the agreement between the experimental and computed pressure distributions is good. Such discrepancies as do exist can be charged to the limitations of the method of computation (which, for one thing, ignores any viscous effects) and possibly to small construction errors in the profiles of the experimental models.

CONCLUSIONS

The stalling characteristics of cambered airfoil sections as affected by the NACA 0010 and 64A010 basic thickness distribution were investigated at low speeds. The amounts of camber were those for design lift coefficients of 0.3 and 0.8. From data obtained at Reynolds numbers of 3.7×10^6 and 5.2×10^6 the following conclusions can be drawn:

1. The maximum section lift coefficients of the four-digit sections were greater than those of the 64A-series sections for all test conditions. The superiority of the four-digit sections diminished with increased amount of camber.

2. The stall of the sections was little affected by the change of thickness distribution, but was significantly affected by camber. Visual observation of tufts attached to the upper surfaces of the models indicated that the stall of the sections cambered for an ideal lift coefficient of 0.3 was the result of separation of flow from the leading edge almost immediately after the appearance of turbulent separation at the trailing edge; whereas, for the sections cambered for an ideal lift coefficient of 0.8, turbulent separation from the trailing edge progressed as far forward as the 70-percent-chord station before laminar separation appeared near the leading edge.

3. The effect of Reynolds number on maximum lift was small for the range investigated.

4. Surface roughness decreased the maximum lift of all the unflapped airfoil sections. This reduction was greater for the sections cambered for a design lift coefficient of 0.3 than for those cambered for a design lift coefficient of 0.8. Roughness reduced the maximum lift of the flapped four-digit-series sections, but showed no consistent effect on the flapped 64A-series sections.

5. The increment of maximum lift produced by a simulated split flap deflected 60° was greater for the four-digit-series airfoils than for the 64A series. For either series, the increment of maximum lift produced by the flap was greater for the greater amount of camber.

Ames Aeronautical Laboratory,
National Advisory Committee for Aeronautics,
Moffett Field, Calif., May 12, 1950.

REFERENCES

1. Nitzberg, Gerald E., and Crandall, Stewart: A Study of Flow Changes Associated With Airfoil Section Drag Rise at Supercritical Speeds. NACA TN 1813, 1949.

2. Abbott, Ira H., von Doenhoff, Albert E., and Stivers, Louis S., Jr.: Summary of Airfoil Data. NACA Rep. 824, 1945.

3. Loftin, Laurence K., Jr.: Theoretical and Experimental Data for a Number of NACA 6A-Series Airfoil Sections. NACA Rep. 903, 1948.

4. Allen, H. Julian, and Vincenti, Walter G.: Wall Interference in a Two-Dimensional-Flow Wind Tunnel, with Consideration of the Effect of Compressibility. NACA Rep. 782, 1944.

5. McCullough, George B., and Gault, Donald E.: Boundary-Layer and Stalling Characteristics of the NACA 64A006 Airfoil Section. NACA TN 1923, 1949.

TABLE I.- COORDINATES OF CAMBERED AIRFOIL SECTIONS

NACA 0010
c_{l_i}=0.3, a=1.0

[Stations and ordinates given in percent of airfoil chord]

Upper surface		Lower surface	
Station	Ordinate	Station	Ordinate
0	0	0	0
1.086	1.731	1.414	-1.409
2.310	2.449	2.690	-1.891
4.792	3.429	5.208	-2.481
7.290	4.130	7.710	-2.858
9.796	4.672	10.204	-3.122
14.816	5.460	15.184	-3.442
19.842	5.973	20.158	-3.585
24.870	6.293	25.130	-3.607
29.899	6.459	30.101	-3.543
39.953	6.443	40.047	-3.231
50.000	6.066	50.000	-2.758
60.037	5.409	59.963	-2.197
70.062	4.512	69.938	-1.594
80.072	3.380	79.928	-.992
90.063	1.980	89.937	-.430
95.047	1.144	94.953	-.196
100.000	.105	100.000	-.105

L. E. radius: 1.100. Slope of radius through L. E.: 0.126.

NACA 0010
c_{l_i}=0.8, a=0.8 (modified)

[Stations and ordinates given in percent of airfoil chord]

Upper surface		Lower surface	
Station	Ordinate	Station	Ordinate
0	0	0	0
.774	1.987	1.726	-1.023
1.938	2.948	3.062	-1.260
4.371	4.337	5.629	-1.453
6.857	5.386	8.143	-1.494
9.365	6.235	10.635	-1.465
14.415	7.541	15.585	-1.293
19.488	8.476	20.512	-1.034
24.571	9.139	25.429	-.727
29.657	9.584	30.343	-.396
39.826	9.949	40.174	.281
49.786	9.733	50.214	.909
60.108	9.007	59.892	1.405
70.210	7.776	69.790	1.684
80.312	5.881	79.688	1.595
90.233	3.146	89.767	.778
95.129	1.640	94.871	.322
100.000	.103	100.000	-.103

L. E. radius: 1.100. Slope of radius through L. E.: 0.380.

NACA 64A310
a=1.0

[Stations and ordinates given in percent of airfoil chord]

Upper surface		Lower surface	
Station	Ordinate	Station	Ordinate
0	0	0	0
.399	.873	.601	-.723
.638	1.068	.862	-.858
1.123	1.379	1.377	-1.057
2.353	1.961	2.647	-1.403
4.837	2.759	5.163	-1.847
7.332	3.436	7.668	-2.164
9.832	3.970	10.168	-2.420
14.842	4.819	15.158	-2.809
19.859	5.464	20.141	-3.076
24.879	5.946	25.121	-3.262
29.902	6.294	30.098	-3.378
34.927	6.513	35.073	-3.423
39.952	6.601	40.048	-3.389
44.977	6.536	45.023	-3.252
50.000	6.334	50.000	-3.030
55.021	6.030	54.979	-2.746
60.039	5.627	59.961	-2.415
65.053	5.142	64.947	-2.052
70.063	4.584	69.937	-1.668
75.069	3.964	74.931	-1.280
80.070	3.296	79.930	-.908
85.065	2.582	84.935	-.580
90.056	1.836	89.944	-.286
95.038	1.014	94.962	-.065
100.000	.021	100.000	-.021

L. E. radius: 0.687. T. E. radius: 0.023. Slope of radius through L. E.: 0.126.

NACA 64A810
a=0.8 (modified)

[Stations and ordinates given in percent of airfoil chord]

Upper surface		Lower surface	
Station	Ordinate	Station	Ordinate
0	0	0	0
.214	.976	.785	-.526
.428	1.231	1.072	-.597
.881	1.650	1.619	-.686
2.064	2.475	2.936	-.787
4.506	3.716	5.494	-.832
6.984	4.703	8.016	-.811
9.479	5.541	10.521	-.771
14.500	6.902	15.500	-.658
19.543	7.968	20.457	-.526
24.601	8.795	25.399	-.383
29.668	9.420	30.332	-.232
34.742	9.857	35.258	-.085
39.820	10.107	40.180	.123
44.900	10.150	45.100	.364
49.977	10.005	50.023	.637
55.049	9.693	54.951	.917
60.114	9.225	59.886	1.187
65.169	8.612	64.831	1.426
70.215	7.850	69.785	1.610
75.252	6.932	74.748	1.710
80.300	5.819	79.700	1.657
85.292	4.441	84.708	1.331
90.204	3.004	89.796	.920
95.104	1.512	94.896	.450
100.000	.021	100.000	-.021

L. E. radius: 0.687. T. E. radius: 0.023. Slope of radius through L. E.: 0.380.

NACA

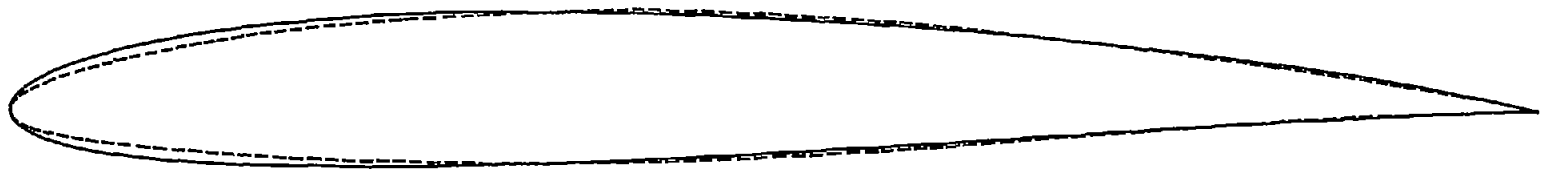

$c_{l_i} = 0.3$, NACA $a = 1.0$ mean line

$c_{l_i} = 0.8$, NACA $a = 0.8$ (modified) mean line

—— NACA four-digit series
---- NACA 64A- series

Figure 1.—Comparison of the four airfoil sections.

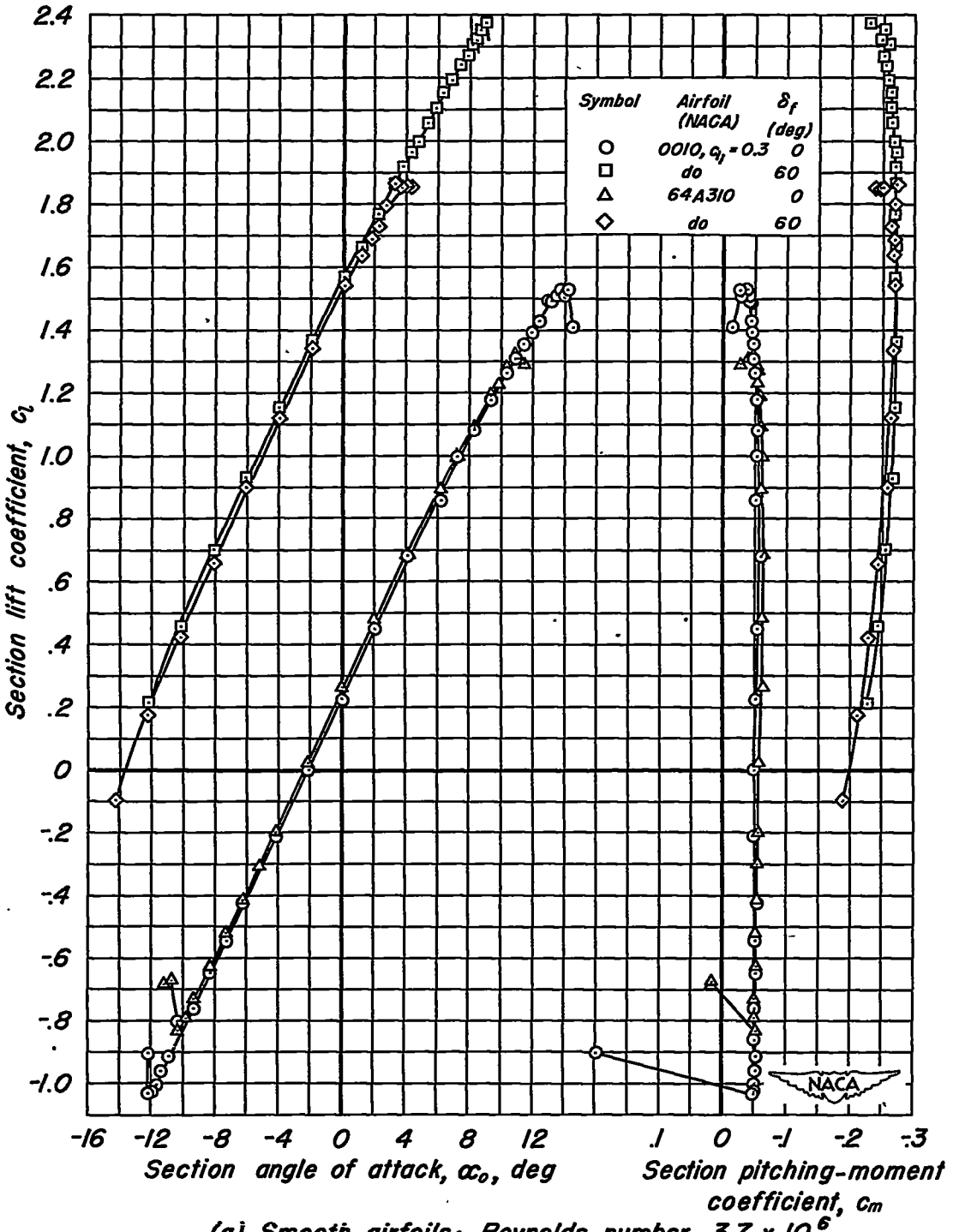

(a) Smooth airfoils; Reynolds number, 3.7×10^6.

Figure 2.— Section lift and pitching-moment characteristics of the two models cambered for a design lift coefficient of 0.3.

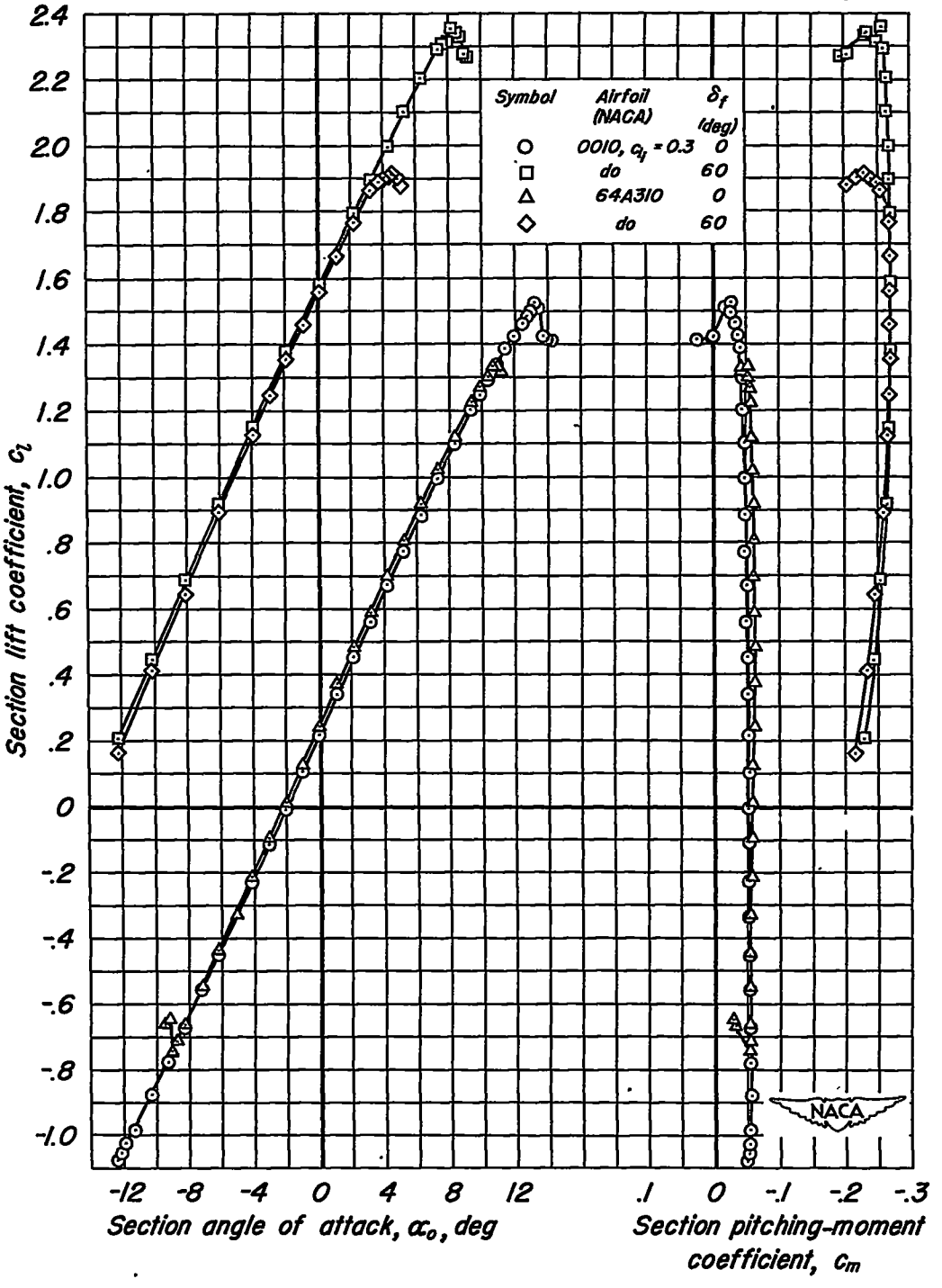

(b) Smooth airfoils; Reynolds number, 5.2×10^6.

Figure 2.— Continued.

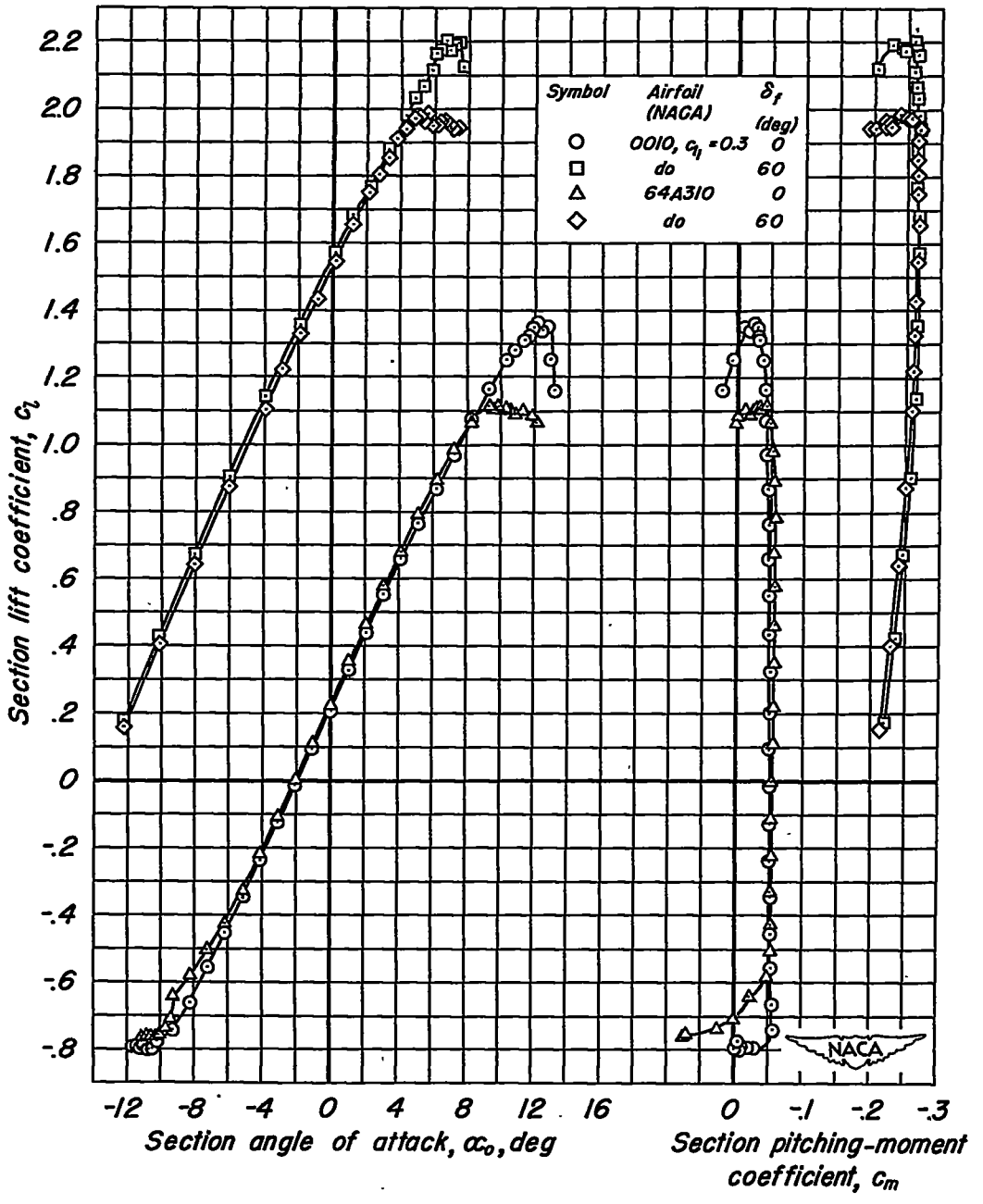

(c) Airfoils with leading-edge roughness; Reynolds number, 5.2×10^6.

Figure 2.—Concluded.

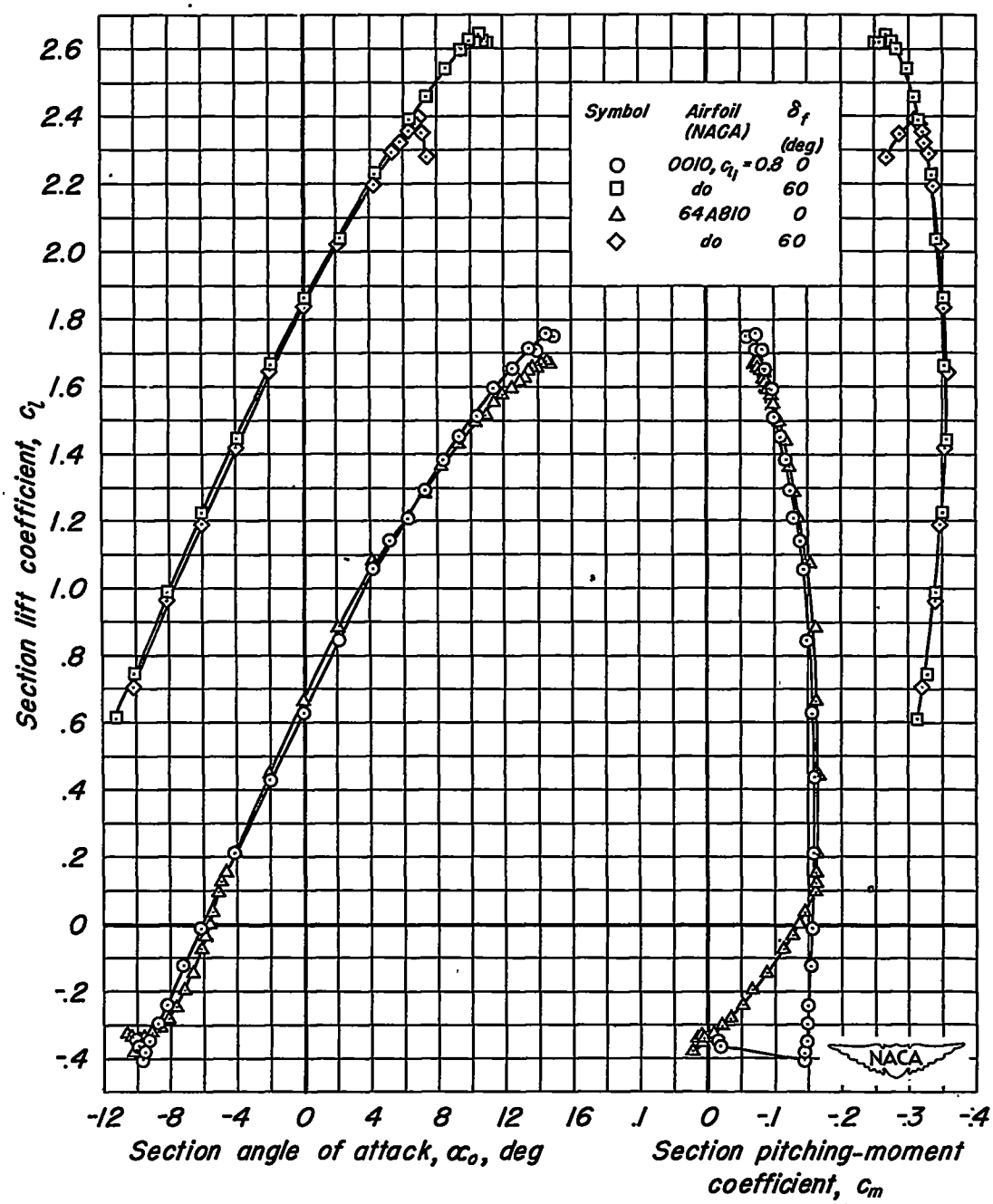

(a) Smooth airfoils; Reynolds number 3.7×10^6.

Figure 3.—Section lift and pitching-moment characteristics of the two models cambered for a design lift coefficient of 0.8.

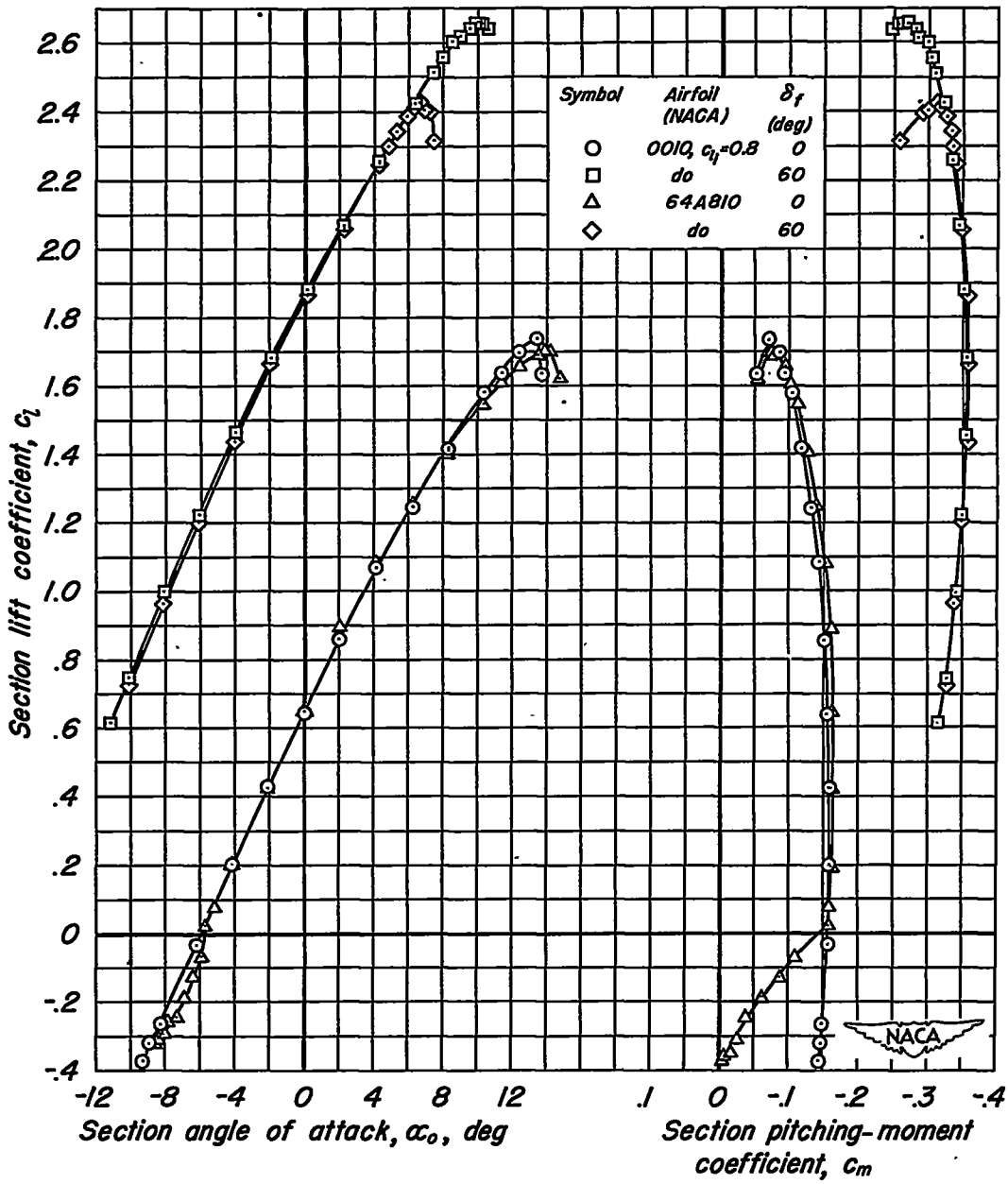

(b) Smooth airfoils; Reynolds number, 5.2×10^6.

Figure 3.— Continued.

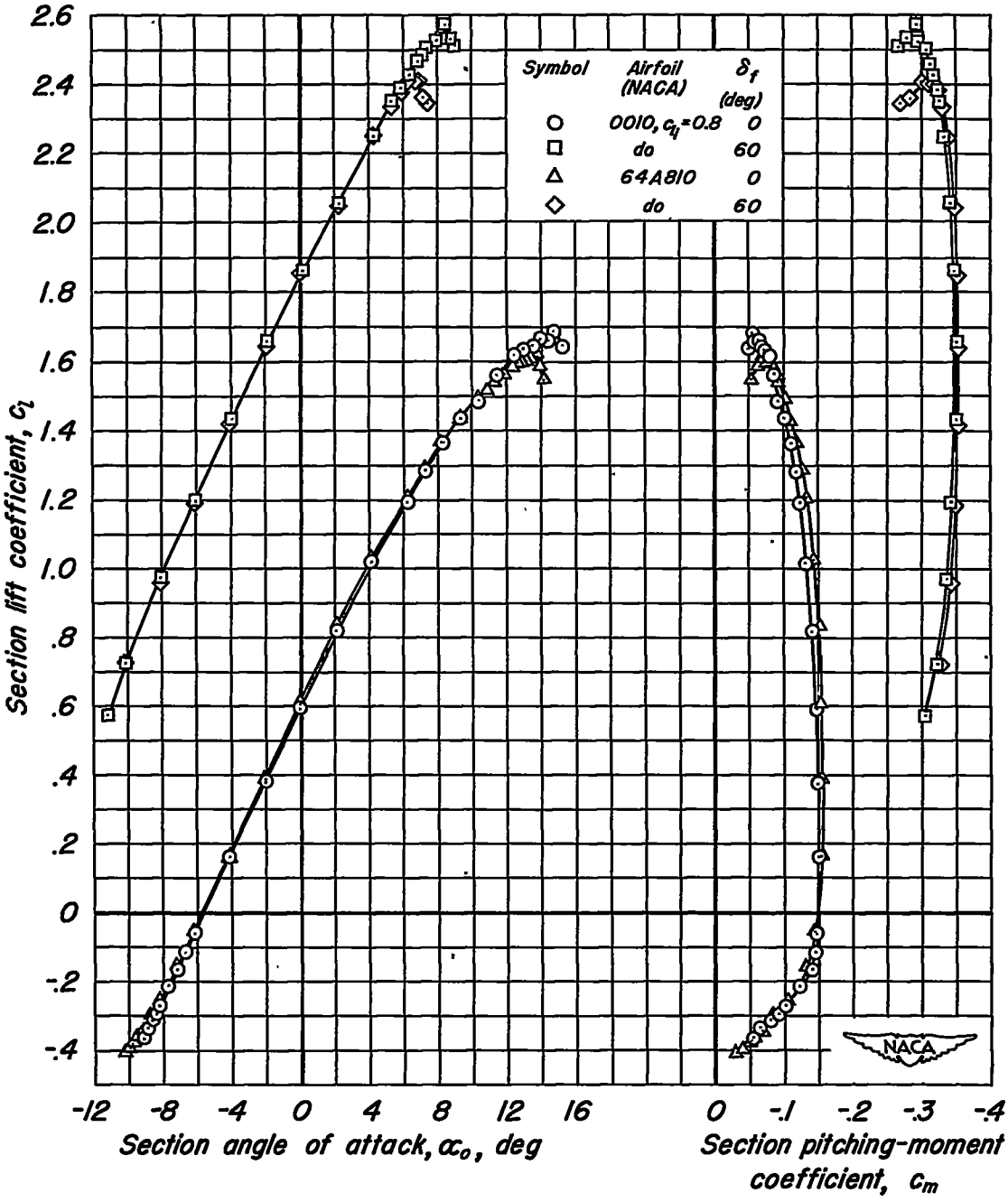

(c) Airfoils with leading-edge roughness; Reynolds number, 5.2 x 10^6.

Figure 3.— Concluded.

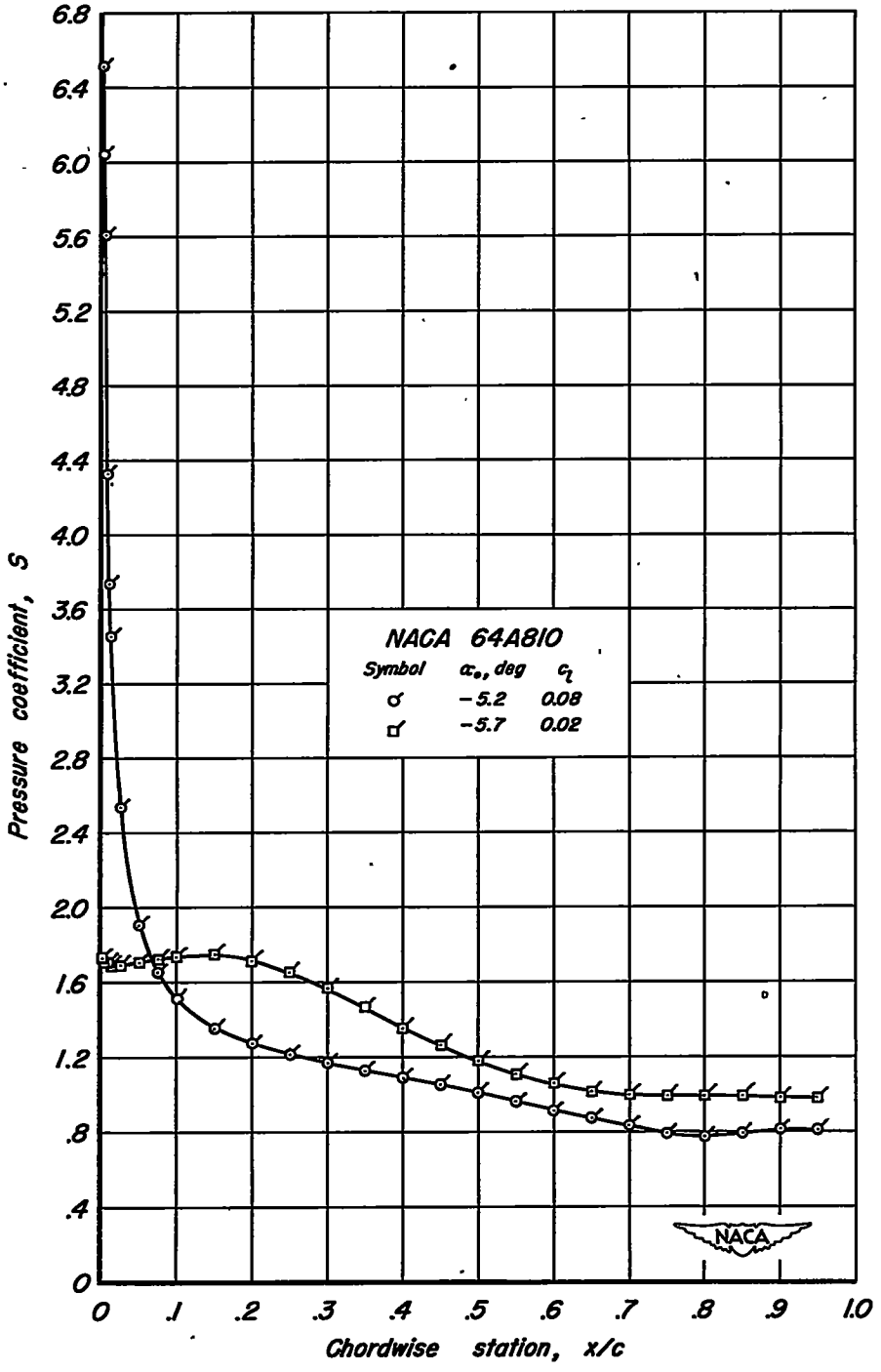

Figure 4.—Lower-surface pressure distribution for the NACA 64A810 airfoil. Reynolds number, 5.2 x 10⁶.

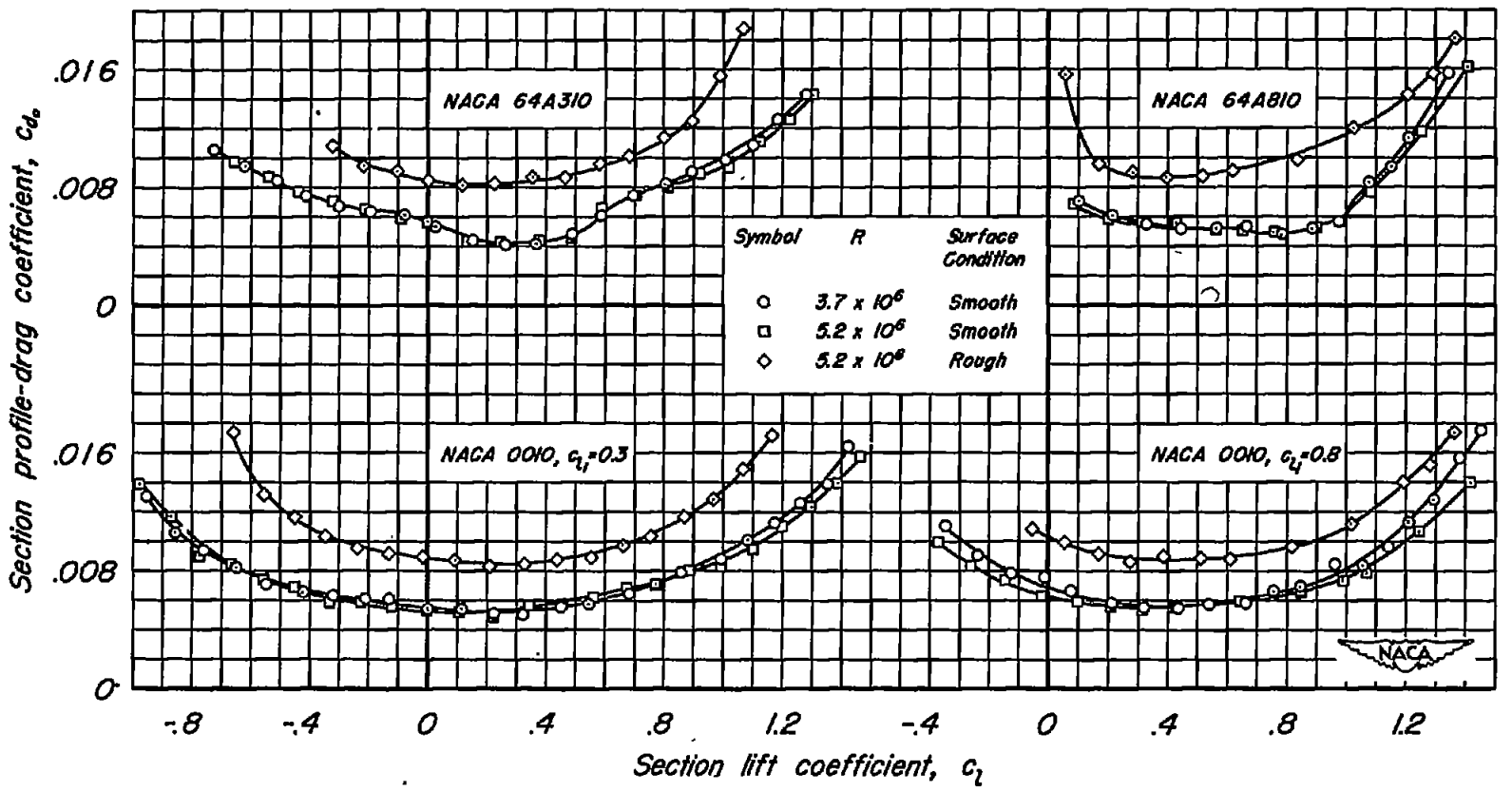

Figure 5.- Section profile-drag characteristics of the four airfoils.

Flagged symbols indicate lower surface.

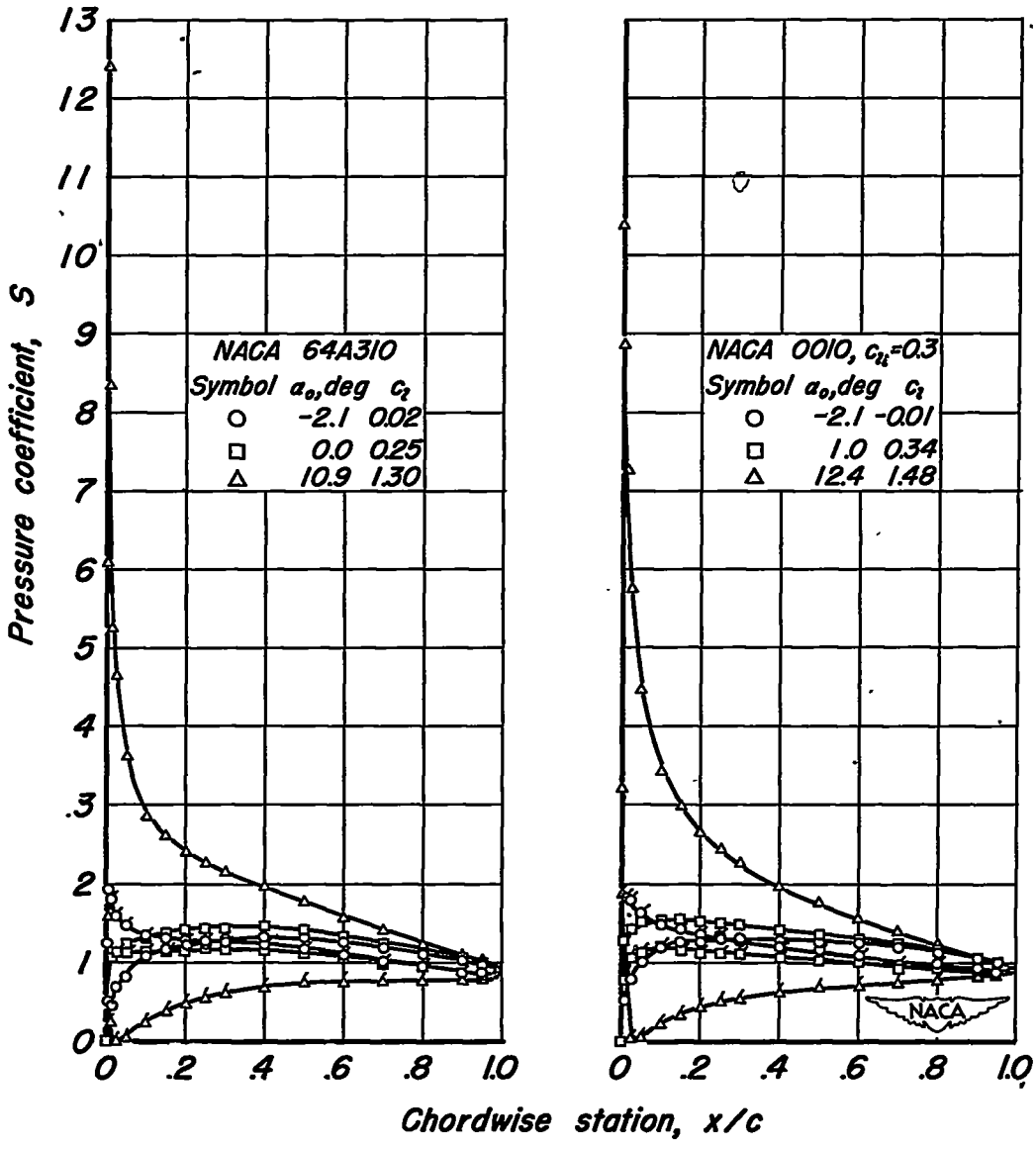

(a) Airfoils cambered for a design lift coefficient of 0.3.

Figure 6.— Representative pressure distributions of the four cambered airfoils. Reynolds number, 5.2 x 10^6.

Flagged symbols indicate lower surface.

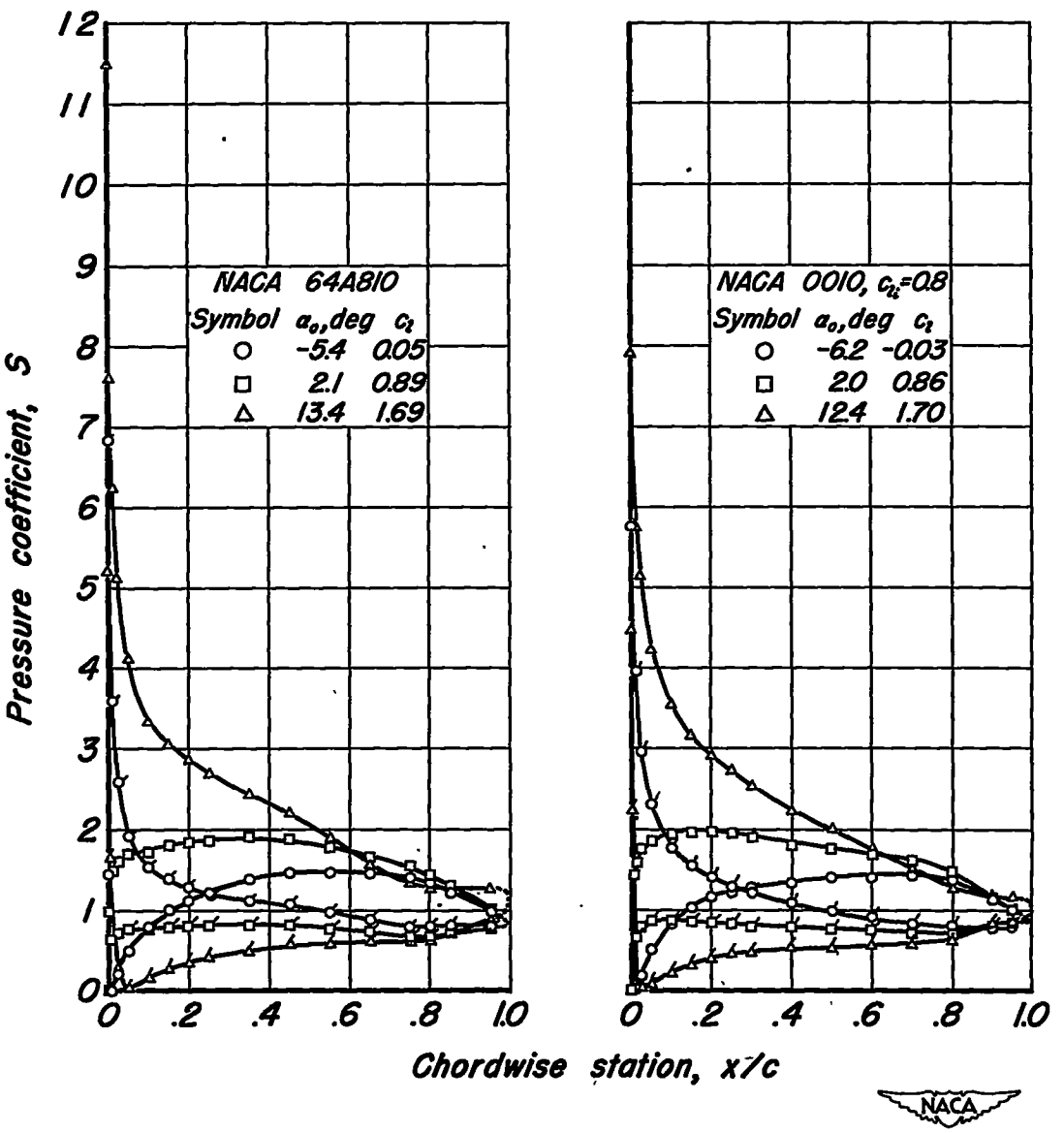

(b) Airfoils cambered for a design lift coefficient of 0.8.

Figure 6.— Concluded.

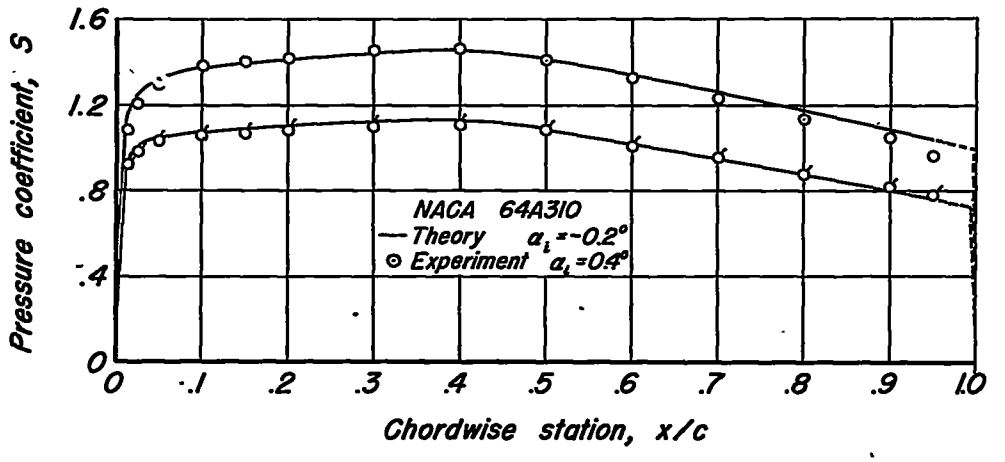

Flagged symbols indicate lower surface.

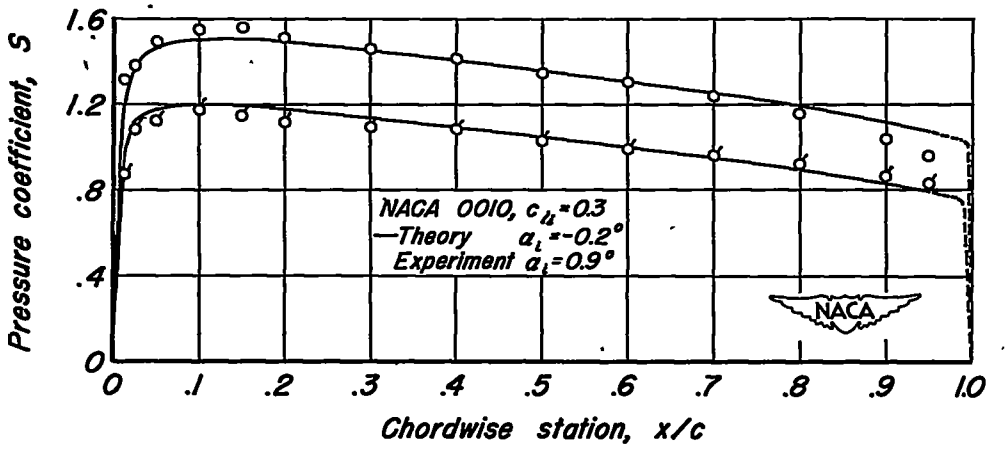

(a) Airfoils cambered for a design lift coefficient of 0.3.

Figure 7.— Comparison of the theoretical and experimental pressure distribution corresponding to the design lift coefficient.

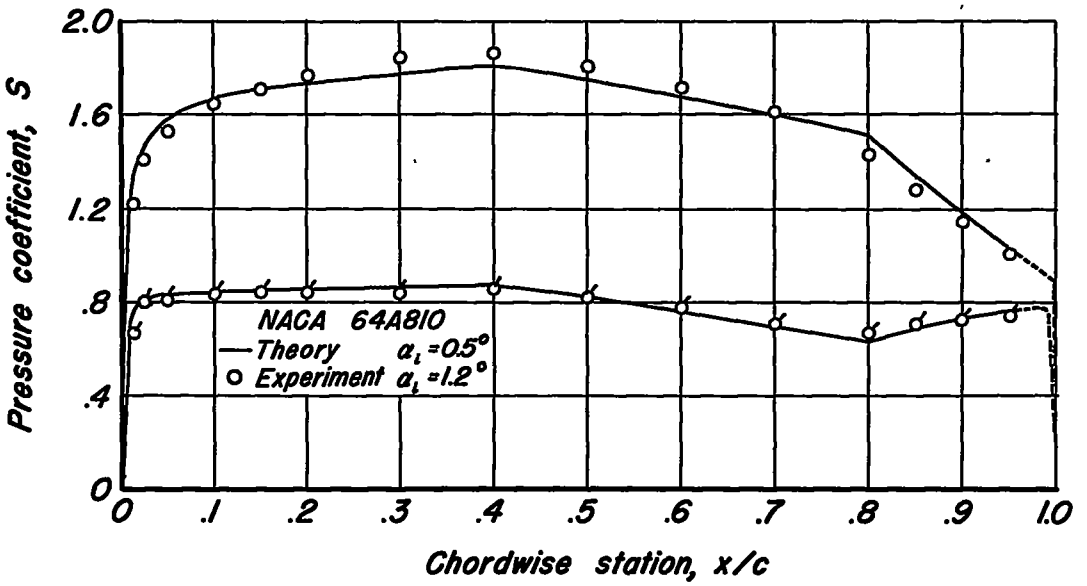

Flagged symbols indicate lower surface.

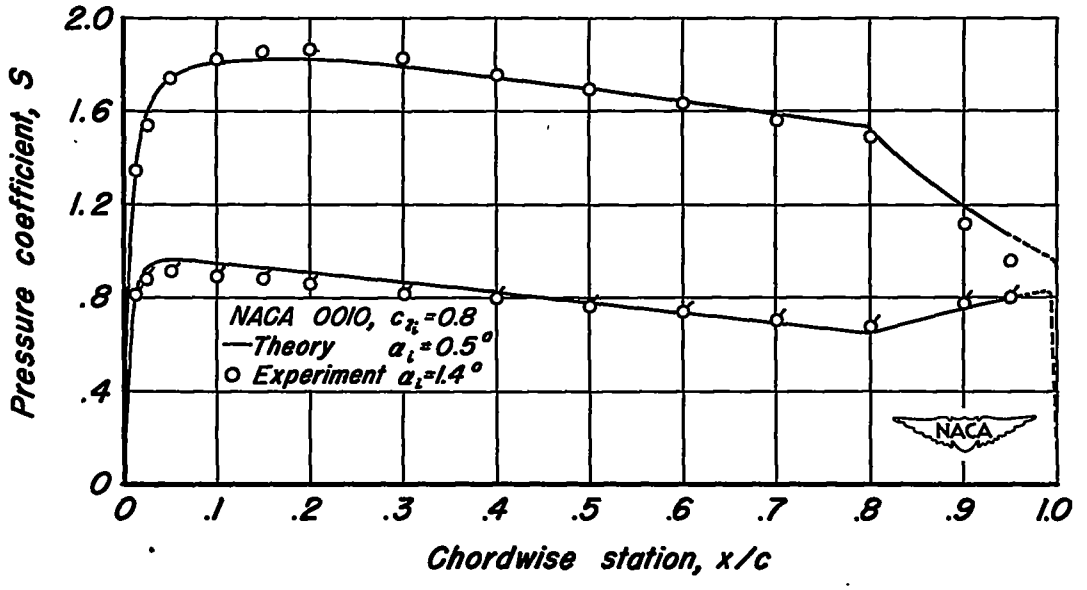

(b) Airfoils cambered for a design lift coefficient of 0.8.

Figure 7.— Concluded.

NACA-Langley - 8-31-50 - 925